Analytical Derivative Approaches for Vibro-Polaritionic Structures and Properties

Xunkun Huang and WanZhen Liang[a)]

State Key Laboratory of Physical Chemistry of Solid Surfaces,
Collaborative Innovation Center of Chemistry for Energy Materials,
Fujian Provincial Key Laboratory of Theoretical and Computational Chemistry,
and Department of Chemistry, College of Chemistry and Chemical Engineering,
Xiamen University, Xiamen 361005, P. R. China.

Vibro-polaritons are hybrid light-matter states that arise from the strong coupling between molecular vibrations and the electromagnetic field in an optical resonator. The study of the related phenomena has spurred the emergence of a new field, now known as polaritonic chemistry. To fully understand the precise mechanisms underpinning polaritonic chemistry and provide a deeper understanding of the underlying quantum mechanical processes, developing useful theoretical models and advanced computational frameworks to describe and predict the behavior of these hybrid states is crucial. Here we present advanced analytical energy derivative approaches within the framework of the cavity Born-Oppenheimer density functional theory (CBO-DFT) to efficiently calculate the vibro-polaritonic spectra and explore the critical points on the cavity potential energy surface. We not only demonstrate the formulation and implementation of analytical energy gradient and Hessian as well as the infrared (IR) and Raman scattering spectral intensities into the electronic structure software package, but also proposes a classical model that helps us to understand the spectral signatures. As a first application of our developed codes, we study the IR and Raman scattering spectra of acetone in the cavity.

[a)]Electronic mail: liangwz@xmu.edu.cn

I. INTRODUCTION

When few (many) molecules are placed in a nano- (micro-)cavity, the photon quasi-particles in the cavity will greatly enhance the intrinsic coupling between the molecular electrons/vibrations and the quantized electromagnetic field, resulting in the formation of polariton states and the modification of the physical and chemical properties.[1–6] In the vibrational strong coupling (VSC) regime in which the light-matter coupling is strong enough to exceed the sum of the two parts' dissipation rates, the coupling of cavity photon and molecular vibrations creates the vibro-polariton states, which have exhibited modified properties compared to the uncoupled states,[7–10] such as enhancing[11,12] or suppressing[13,14] the rate of chemical reactions, controlling the reaction selectivity.[15–17] In experiments, the formation of vibro-polaritons can be detected by vibrational spectroscopy, including linear infrared (IR) spectra,[18] nonlinear 2-dimensional IR,[19–23] and Raman scattering spectra.[24–27]

The research in this field is advancing rapidly, with experimental techniques being developed to predict and control the formation of vibro-polaritons and with theoretical models and computational frameworks being developed to describe and predict the behavior of these hybrid states.[28–35] The cavity Born-Oppenheimer approaximation (CBOA) provides a theoretical framework to study VSC, in which the nuclei and photon are treated on the equal footing so that spans the cavity potential energy surfaces (CPES).[36,37] Currently there are two types of theoretical methods based on the CBOA which focus on the energy representation. The time-dependent dynamics methods[38,39] are beyond the subject of this manuscript. The first type (denoted as *ab initio* CBO in this manuscript) focuses on solving electronic eigenstates, including QEDFT,[40] CBO-HF,[41,42] and CBO-CC.[43] Among these methods, the photon displacement coordinate is added as an external parameter like nuclear coordinates, and light-matter interaction is treated self-consistently. Therefore the photon-electron correlation has been taken into account. Another types of methods (denoted as perturbative CBO in this manuscript) include crude CBOA[44] and CBO-PT.[45,46] In these methods, the light-matter interaction operator is projected onto the bare electronic eigenstates, which can be obtained by conventional quantum chemistry calculations. And the photon-electron correlation is added perturbatively. A main advantage of perturbative CBO methods is that one can just relay on the existing quantum chemistry code, as long as the molecular vibrational normal mode and light-matter interaction matrix elements can be calculated.

While for *ab initio* CBO methods, the photon displacement coordinate and the light-matter interaction have to be explicitly added in the electronic structure software package.

Beyond the energy calculations, one would like to optimize molecular geometries, find reaction pathways, calculate thermal and spectroscopic properties and so on with respect to the CPES. This urges us to implement the analytical energy derivatives with respect to the nuclear, perturbed electric field and photonic degrees of freedom (DOF) into the electronic structure package.[47,48] The analytical gradient of CBO-HF energy has been formulated and used to calculate *ab initio* vibro-polaritonic spectra by Kowalewski et al.[42] However the required Hessian in their spectral calculation was obtained by numerically differentiating the energy gradient, and the geometries of molecules in the cavity were not re-optimized. Furthermore, the HF method largely overestimates the harmonic frequencies compared with the corresponding experimental fundamentals. Aiming at solving these issues, in this work, we first combine the CBOA with the density functional theory (DFT) and develop CBO-DFT approach. Then we formulate the analytical gradient and Hessian of CBO-DFT energy as well as the nuclear and photonic derivatives of dipole and polarizability. The successful implementation of analytical derivatives enables us to effectively calculate the linear IR and Raman scattering spectra of vibro-polaritons. The procedure of geometry optimization on the CPES will also be implemented so that one can analysis the critical points on the CPES. Thanks to the explicit expression of analytical derivatives, we also present a model Hessian with respect to two coupled harmonic oscillators in order to understand the features in the vibro-polaritonic spectra. The acetone molecule is selected as an example to show all the features of vibro-polaritonic spectra.

The manuscript is arranged as follows. In Sec.II, we present the expressions of CBO-DFT energy, energy gradient, and Hessian, and we also rationalize the procedure of calculating the frequencies and spectral intensities of vibro-polaritons. In Sec.III, we show geometry optimization on the CPES, the model Hessian that helps us to understand the features of vibro-polaritonic spectra, and the *ab initio* vibro-polaritonic spectra of acetone calculated within the framework of the CBO-DFT. Finally, the concluding remarks are summarized in Sec.IV.

II. THEORY

In this manuscript, the subscript A is the index of nuclei, and i the electrons. n represents the Cartesian components which can be $\{x, y, z\}$. $\{p, q, \ldots\}$ index molecular orbitals (MO), $\{i, j, \ldots\}$ the occupied MOs, and $\{\mu, \nu, \ldots\}$ the atomic orbitals (AO). The superscript x represents nuclear derivative, and q the derivative with respect to photon displacement coordinate. The superscripts bracketed with '[]' refer to the explicit derivatives excluding the contributions from orbital rotations Θ. The detailed derivations of analytical derivatives shown in this section are presented in the supplementary material.

A. CBO-DFT Energy and Gradients

The usual starting point of polaritonic chemistry is the Pauli-Fierz Hamiltonian (in the length gauge and dipole approximation)[49]

$$\hat{H} = \hat{T}_{\text{nuc}} + \hat{H}_{\text{e}} + \omega_{\text{c}}\hat{b}^\dagger\hat{b} - \sqrt{\frac{\omega_{\text{c}}}{2}}(\boldsymbol{\lambda}\cdot\hat{\boldsymbol{\mu}})(\hat{b}^\dagger + \hat{b}) + \frac{1}{2}(\boldsymbol{\lambda}\cdot\hat{\boldsymbol{\mu}})^2, \tag{1}$$

$$= \hat{T}_{\text{nuc}} + \hat{H}_{\text{e}} + \frac{\hat{p}^2}{2} + \frac{1}{2}\omega_{\text{c}}^2\hat{q}^2 - \omega_{\text{c}}(\boldsymbol{\lambda}\cdot\hat{\boldsymbol{\mu}})\hat{q} + \frac{1}{2}(\boldsymbol{\lambda}\cdot\hat{\boldsymbol{\mu}})^2. \tag{2}$$

$\hat{T}_{\text{nuc}} + \hat{H}_{\text{e}}$ constitutes the molecular Hamiltonian in vacuum. $\omega\hat{b}^\dagger\hat{b}$ or $\frac{1}{2}(\hat{p}^2 + \omega_{\text{c}}^2\hat{q}^2)$ is the photonic Hamiltonian (we only consider single mode). The last term $\frac{1}{2}(\boldsymbol{\lambda}\cdot\hat{\boldsymbol{\mu}})^2$ is the so-called dipole self-energy operator, and it ensures the light-matter system to have a ground state.[50] $\hat{\boldsymbol{\mu}} = \sum_A Z_A\hat{\mathbf{R}}_A - \sum_i \hat{\mathbf{r}}_i$ is the molecular dipole operator, and $\boldsymbol{\lambda} = \sqrt{\frac{\hbar}{\varepsilon_0 V}}\mathbf{e}$ is the coupling vector, in which its magnitude represents the strength of cavity electric field, and $\mathbf{e}$ is the unit vector representing the transverse polarization direction. The remaining term $-\sqrt{\frac{\omega_{\text{c}}}{2}}(\boldsymbol{\lambda}\cdot\hat{\boldsymbol{\mu}})(\hat{b}^\dagger + \hat{b})$ or $-\omega_{\text{c}}(\boldsymbol{\lambda}\cdot\hat{\boldsymbol{\mu}})\hat{q}$ describes the light-matter interaction.

In the VSC regime, the cavity electromagnetic mode is coupled to molecular vibrational degrees of freedom. The CBOA provides a theoretical framework to describe VSC. At this stage, the nuclear and photonic kinetic operators are separated from the PF Hamiltonian, and we treat the nuclear coordinates and photon displacement coordinate as external parameters instead of operators. This results in the CBO Hamiltonian

$$\hat{H}_{\text{CBO}} = \hat{H}_{\text{e}}(\mathbf{R}) + \frac{1}{2}\omega_{\text{c}}^2 q^2 - \omega_{\text{c}}(\boldsymbol{\lambda}\cdot\hat{\boldsymbol{\mu}})q + \frac{1}{2}(\boldsymbol{\lambda}\cdot\hat{\boldsymbol{\mu}})^2, \tag{3}$$

and also defines the CPES, $E_{\text{CBO}}(\mathbf{R}, q)$.

In this work, we include the DFT exchange-correlation (XC) functional in the electronic Hamiltonian $\hat{H}_{\mathrm{e}}$. The formalism of the adopted XC functional is just the standard one that employed in conventional quantum chemistry code. This treatment neglects the electron-photon correlation in the functional, but we also point that the electronic response to the cavity photon is treated self-consistently in this work. Similar to the CBO-HF ansatz, the electronic ground state is described by a single determinant of Kohn-Sham orbitals, and the corresponding expression of energy in atomic orbital (AO) representation is[41,49]

$$\begin{aligned} E_{\mathrm{CBO}}(\mathbf{R}, q) = \mathbf{h}\cdot\mathbf{P} + \frac{1}{2}\mathbf{P}\cdot\mathbf{\Pi}\cdot\mathbf{P} + E_{\mathrm{xc}} + V_{\mathrm{nuc}} + \frac{1}{2}\omega_{\mathrm{c}}^2 q^2 \\ - \omega_{\mathrm{c}} q \boldsymbol{\lambda}\cdot\boldsymbol{\mu} + \frac{1}{2}(\boldsymbol{\lambda}\cdot\boldsymbol{\mu})^2 + \mathbf{q}\cdot\mathbf{P} - \frac{1}{2}\mathbf{P}\cdot(\mathbf{dPd}). \end{aligned} \tag{4}$$

Here we define the matrix $d_{\mu\nu} = \sum_n \lambda_n M_{n,\mu\nu}$ in which $\mathbf{M}_n$ is the dipole matrix of n-component, and also define the matrix $q_{\mu\nu} = \frac{1}{2}\sum_{mn}\lambda_m Q_{mn,\mu\nu}\lambda_n$ in which $\mathbf{Q}_{mn}$ is the quadrupole matrix. $\mu_n = \sum_A Z_A R_{A,n} - \mathbf{P}\cdot\mathbf{M}_n$ is the total dipole moment of molecule in n-direction. The CBO-DFT Fock matrix is

$$\mathbf{F} = \mathbf{h} + \mathbf{\Pi}\cdot\mathbf{P} + \mathbf{V}_{\mathrm{xc}}(\mathbf{P}) + (\omega_{\mathrm{c}} q - \boldsymbol{\lambda}\cdot\boldsymbol{\mu}_{\mathrm{nuc}})\mathbf{d} + \mathbf{q} + \mathbf{d}(\mathbf{d}\cdot\mathbf{P}) - \mathbf{dPd}. \tag{5}$$

Because CBO-DFT wavefunction is variational, the nuclear gradients of CBO-DFT energy can be derived by the Lagrangian approach.[51] The CBO-DFT Lagrangian is defined as $L_{\mathrm{CBO}} = E_{\mathrm{CBO}} - \sum_{pq}\varepsilon_{pq}(S_{pq} - \delta_{pq})$. The derivative of CBO energy is therefore the partial derivative of energy Lagrangian

$$\begin{aligned} E^x_{\mathrm{CBO}} &= \frac{\mathrm{d}E_{\mathrm{CBO}}}{\mathrm{d}x} = \frac{\partial L_{\mathrm{CBO}}}{\partial x} \\ &= \mathbf{h}^{[x]}\cdot\mathbf{P} + \frac{1}{2}\mathbf{P}\cdot\mathbf{\Pi}^{[x]}\cdot\mathbf{P} + E^{[x]}_{\mathrm{xc}} + V^{[x]}_{\mathrm{nuc}} - \mathbf{W}\mathbf{S}^{[x]} \\ &\quad + (\boldsymbol{\lambda}\cdot\boldsymbol{\mu} - \omega_{\mathrm{c}} q)(\boldsymbol{\lambda}\cdot\boldsymbol{\mu}^{[x]}_{\mathrm{nuc}} - \mathbf{d}^{[x]}\cdot\mathbf{P}) + \mathbf{q}^{[x]}\cdot\mathbf{P} - \mathbf{P}\cdot(\mathbf{dPd}^{[x]}), \end{aligned} \tag{6}$$

in which $W_{\mu\nu} = \sum_i C_{\mu i}\varepsilon_i C_{\nu i} = (\mathbf{PFP})_{\mu\nu}$ and it is called energy weighted density matrix. Since there is one new dimension, the photon displacement coordinate q, the gradient with respect to it is also required. The Lagrangian approach is also applied, but in this case the constraint term does not explicitly depend on q. The expression of photonic gradient is

$$E^q_{\mathrm{CBO}} = \frac{\partial L_{\mathrm{CBO}}}{\partial q} = \omega_{\mathrm{c}}^2 q - \omega_{\mathrm{c}}\boldsymbol{\lambda}\cdot\boldsymbol{\mu}. \tag{7}$$

B. CBO-DFT Hessian

The second derivative of CBO-DFT energy is essential for calculating harmonic vibrational spectra, and it is important for geometry optimization on the CPES. The expression of Hessian is obtained by directly differentiating on the gradient. The photon-photon Hessian and photon-molecule Hessian are easy to get:

$$E^{qq}_{\mathrm{CBO}} = \omega_{\mathrm{c}}^2 - \omega_{\mathrm{c}}\boldsymbol{\lambda}\cdot\boldsymbol{\mu}^q, \tag{8}$$

$$E^{qx}_{\mathrm{CBO}} = -\omega_{\mathrm{c}}\boldsymbol{\lambda}\cdot\boldsymbol{\mu}^x. \tag{9}$$

In both parts, the derivatives of total dipole are involved. The nuclear derivative of dipole is $\mu_n^x = \sum_A Z_A R_{A,n}^{[x]} - \mathbf{M}_n\cdot\mathbf{P}^x - \mathbf{M}_n^{[x]}\cdot\mathbf{P}$ and photonic derivative of dipole is $\mu_n^q = -\mathbf{M}_n\cdot\mathbf{P}^q$. And the expression of Hessian with respect to nuclear displacement is

$$\begin{aligned} E^{xy}_{\mathrm{CBO}} = {} & \mathbf{h}^{[xy]}\cdot\mathbf{P} + \frac{1}{2}\mathbf{P}\cdot\boldsymbol{\Pi}^{[xy]}\cdot\mathbf{P} + E_{\mathrm{xc}}^{[xy]} + V_{\mathrm{nuc}}^{[xy]} \\ & - (\boldsymbol{\lambda}\cdot\boldsymbol{\mu} - \omega_{\mathrm{c}}q)\mathbf{d}^{[xy]}\cdot\mathbf{P} + (\boldsymbol{\lambda}\cdot\boldsymbol{\mu}_{\mathrm{nuc}}^{[y]} - \mathbf{d}^{[y]}\cdot\mathbf{P})(\boldsymbol{\lambda}\cdot\boldsymbol{\mu}_{\mathrm{nuc}}^{[x]} - \mathbf{d}^{[x]}\cdot\mathbf{P}) \\ & + \mathbf{q}^{[xy]}\cdot\mathbf{P} - \mathbf{P}\cdot(\mathbf{d}\mathbf{P}\mathbf{d}^{[xy]}) - \mathbf{P}\cdot(\mathbf{d}^{[y]}\mathbf{P}\mathbf{d}^{[x]}) \\ & + \mathbf{F}^{[x]}\cdot\mathbf{P}^y - \mathbf{W}^y\cdot\mathbf{S}^{[x]} - \mathbf{W}\cdot\mathbf{S}^{[xy]}. \end{aligned} \tag{10}$$

The derivative of energy weighted density matrix is

$$\mathbf{W}^y = \mathbf{P}^y\mathbf{F}\mathbf{P} + \mathbf{P}\mathbf{F}\mathbf{P}^y + \mathbf{P}\mathbf{F}^y\mathbf{P}, \tag{11}$$

and the Fock matrix derivative is

$$\mathbf{F}^y = \mathbf{F}^{[y]} + \boldsymbol{\Pi}\cdot\mathbf{P}^y + \mathbf{V}_{\mathrm{xc}}(\mathbf{P}^y) + \mathbf{d}(\mathbf{d}\cdot\mathbf{P}^y) - \mathbf{d}\mathbf{P}^y\mathbf{d}. \tag{12}$$

In the above expressions, the derivatives of density matrix $\mathbf{P}^x$ and $\mathbf{P}^q$ are required. To calculate them, the derivative of molecular orbital coefficients or orbital rotations $\Theta^{[x]}$ and $\Theta^{[q]}$ are obtained by solving the coupled-perturbed self-consistent field (CPSCF) equations with respect to nuclear displacement and photonic displacement.[52,53] Besides, the orbital response $\Theta^{[n]}$ to electric field perturbation f_n is also solved, which gives us $\mathbf{P}^n$.

To calculate Raman scattering intensity, the derivative of polarizability is required. The expression of polarizability is $\alpha_{mn} = \frac{\partial\mu_m}{\partial f_n} = -\mathbf{M}_m\cdot\mathbf{P}^n$, in which f_n is the electric field along n-direction. And its derivatives with respect to x and q are $\alpha_{mn}^x = -\mathbf{M}_m\cdot\mathbf{P}^{nx}$ and $\alpha_{mn}^q = -\mathbf{M}_m\cdot\mathbf{P}^{nq}$. Thanks to the $2n+1$ rule, the second derivative of density matrix can be calculated only using the first-order orbital response.[54,55] The details of derivations are shown in the supplementary material.

C. Harmonic Frequency and Spectral Intensity

In this work, the procedure for calculating the harmonic frequencies of vibro-polaritons and the corresponding vibro-polaritonic normal modes is as follows. The Hessian matrix is converted to the mass-weighted Hessian (MWH) matrix: $H_{\mathrm{m},xy} = E^{xy}_{\mathrm{CBO}}/\sqrt{M_x M_y}$, $g_x = E^{qx}_{\mathrm{CBO}}/\sqrt{M_x}$, and $H_{\mathrm{c}} = E^{qq}_{\mathrm{CBO}}$. Note that the "photon mass" is assumed to be 1 a.u. so that we do not show it explicitly. This gives us a MWH matrix with size of $(3N+1)\times(3N+1)$, and the matrix has four blocks

$$\begin{pmatrix} \mathbf{H}_{\mathrm{m}} & \mathbf{g} \\ \mathbf{g}^{\dagger} & \mathbf{H}_{\mathrm{c}} \end{pmatrix}. \tag{13}$$

We first diagonalize the molecule part $\mathbf{H}_{\mathrm{m}}$

$$\mathbf{L}'^{\dagger}\mathbf{D}^{\dagger}\mathbf{H}_{\mathrm{m}}\mathbf{D}\mathbf{L}' = \omega'^{2}_{\mathrm{m}}. \tag{14}$$

Here $\mathbf{D}$ is the projection matrix (following the Eckart conditions[56]) that projects out the translational and rotational normal modes of molecule, and $\mathbf{L}'$ is the mass-weighted vibrational normal coordinate matrix. In this step, we solve $3N-6$ (or $3N-5$ for linear molecules) effective vibrational normal modes of molecule in the cavity that are ready to be mixed with cavity mode (, and the corresponding spectral intensities are calculated if needed). Next we build the unitary matrix

$$\mathbf{U} = \begin{pmatrix} \mathbf{D}\mathbf{L}' & 0 \\ 0 & 1 \end{pmatrix}, \tag{15}$$

and use it to transform the original MWH matrix into an intermediate MWH matrix

$$\tilde{\mathbf{H}} = \mathbf{U}^{\dagger}\begin{pmatrix} \mathbf{H}_{\mathrm{m}} & \mathbf{g} \\ \mathbf{g}^{\dagger} & \mathbf{H}_{\mathrm{c}} \end{pmatrix}\mathbf{U} = \begin{pmatrix} \omega'^{2}_{\mathrm{m},1} & 0 & \dots & g'_1 \\ 0 & \omega'^{2}_{\mathrm{m},2} & \dots & g'_2 \\ \vdots & \vdots & \ddots & \vdots \\ g'_1 & g'_2 & \dots & \omega'^{2}_{\mathrm{c}} \end{pmatrix}, \tag{16}$$

in which $\omega'^{2}_{\mathrm{c}} = E^{qq}_{\mathrm{CBO}}$. Finally we diagonalize $\tilde{\mathbf{H}}$, i.e. $\mathbf{X}^{\dagger}\tilde{\mathbf{H}}\mathbf{X} = \omega^2$, to get the harmonic frequencies of vibro-polaritonic states, and the vibro-polaritonic normal coordinate matrix is $\mathbf{L} = \mathbf{U}\mathbf{X}$.

The IR spectral intensity of vibro-polaritonic mode k is $I_k = |\boldsymbol{\mu}_k|^2$, in which $\boldsymbol{\mu}_k$ is the derivative of total dipole with respect to the vibro-polaritonic normal coordinate Q_k

$$\boldsymbol{\mu}_k = \frac{\partial \boldsymbol{\mu}}{\partial Q_k} = \sum_{A=1}^{3N} \frac{L_{A,k}}{\sqrt{M_A}}\frac{\partial \boldsymbol{\mu}}{\partial R_A} + L_{3N+1,k}\frac{\partial \boldsymbol{\mu}}{\partial q}. \tag{17}$$

The polarizability derivative of normal coordinate Q_k is

$$\alpha_{mn,k} = \frac{\partial \alpha_{mn}}{\partial Q_k} = \sum_{A=1}^{3N} \frac{L_{A,k}}{\sqrt{M_A}} \frac{\partial \alpha_{mn}}{\partial R_A} + L_{3N+1,k} \frac{\partial \alpha_{mn}}{\partial q}. \tag{18}$$

The expression of Raman activity S_k is quite lengthy, and readers can refer to it in the Eq.43 of Ref. 57.

The treatment proposed in this section is due to the following reasons. Because the translational and rotational normal modes that include photon displacement coordinate may not be well-defined, the projection only applies to the molecule part of MWH matrix. And the intermediate MWH matrix $\tilde{\mathbf{H}}$ in Eq.16 gives a clear picture of how each molecular vibration interacts with the cavity mode. Additionally, due to the block form of the intermediate MWH matrix, we can build the MWH matrix of molecular ensembles by simply duplicating the effective frequencies and corresponding couplings of molecule, and diagonalize the matrix to calculate the vibrational spectra of molecular ensembles.

III. RESULTS AND DISCUSSIONS

A. Implementation

The CBO-DFT method and its analytical derivative (including gradient and Hessian) are implemented in a local version of Q-Chem package.[58] The procedures of geometry optimization on the CPES, including full optimization and optimization of q with fixed nuclear configuration, are also implemented based on the libopt3 driver.

The full geometry optimization on the CPES requires a mixed coordinate definition, in which the molecule part uses internal coordinate and the photon displacement coordinate is another part. Since the CPES along the q direction is usually much smoother than along the nuclear DOFs, quasi-Newton methods (e.g. BFGS algorithm) are recommended. A brief description of our geometry optimization scheme is presented in the supplementary material. Fig.1 shows geometry optimization of HF molecule in the cavity. The theoretical level of CPES is B3LYP[59]/aug-cc-pVDZ[60], and the strength of coupling vector $\lambda = 0.05$ (in atomic unit, as $1\,\text{a.u.} = 1\,\sqrt{m_\text{e}}E_\text{h}/e\hbar$) with the direction parallel to the H−F bond. The initial bond length and q are $0.8\,\text{Å}$ and $-4.9\,\text{a.u.}$ respectively. With an exact initial Hessian (orange line) or guess initial Hessian (blue line), the full geometry optimizations all converge

to the local minimum, and convergence is faster using the exact initial Hessian.

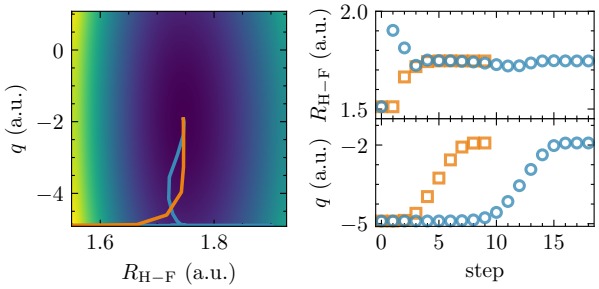

FIG. 1. Left panel displays the trajectories of geometry optimization of HF molecule on the CPES. Right panel displays the H−F bond length and the value of q varied with the number of optimization steps. Orange and blue colors represent the geometry optimization using exact and approximate initial Hessian, respectively.

B. Understanding Vibro-Polaritonic Spectra from Model Hessian

Before presenting the calculated vibro-polaritonic spectra, we can have a basic understanding of them by looking into the formalism of CBO-DFT (which also applies for CBO-HF) and linear response theory of vibro-polariton. The framework of *ab initio* vibro-polaritonic spectra was introduced by Flick et al.,[40] in which the contribution of $\boldsymbol{\mu}^q$ to the cavity frequency and spectral intensity was explicitly considered. Physical insight into the cavity frequency shift and asymmetry in vibro-polaritonic spectra via the perturbative CBO approach were also presented in Ref. 44,46. Here, we show the physical nature of $\boldsymbol{\mu}^q$ from the perspective of molecular property theory. And we propose a model Hessian to show how vibro-polaritonic frequencies and spectral intensities vary with the strength of $\boldsymbol{\lambda}$.

$\boldsymbol{\mu}^q$ is a very important quantity in *ab initio* vibro-polaritonic spectra. In fact, $\boldsymbol{\mu}^q$ shares a similar expression with polarizability: $\mu_n^q = -\mathbf{M}_n \cdot \mathbf{P}^q$ and $\alpha_{mn} = -\mathbf{M}_m \cdot \mathbf{P}^n$. In addition, in the coupled-perturbed self-consistent field equations $E^{\Theta\Theta}_{\mathrm{CBO}} \cdot \Theta^{[n]} = -\mathbf{L}^{[n]}_{\mathrm{vo}}$ and $E^{\Theta\Theta}_{\mathrm{CBO}} \cdot \Theta^{[q]} = -\mathbf{L}^{[q]}_{\mathrm{vo}}$, the photonic Lagrangian is $\mathbf{L}^{[q]} = -\omega_{\mathrm{c}} \sum_n \lambda_n \mathbf{M}_n$, and the electric field Lagrangian is $\mathbf{L}^{[n]} = -\mathbf{M}_n$ (the derivation of these equations are shown in the supplemetary material). It is obvious that $\Theta^{[q]} = \omega_{\mathrm{c}} \sum_n \lambda_n \Theta^{[n]}$. Through this analogy we can interpret $\boldsymbol{\mu}^q$ as the "induced dipole" under the action of $\boldsymbol{\lambda}$, and $\boldsymbol{\mu}^q = \omega_{\mathrm{c}} \boldsymbol{\alpha} \cdot \boldsymbol{\lambda}$. $\boldsymbol{\mu}^q$ and $\boldsymbol{\lambda}$ usually have the same direction (i.e. the off-diagonals of polarizability tensor can be ignored). As a result, the value

of ω_c' (Eq.16) is always smaller than ω_c, and the frequency shift $\omega_c'^2 - \omega_c^2$ is approximately $-\omega_c^2(\boldsymbol{\lambda} \cdot \boldsymbol{\alpha} \cdot \boldsymbol{\lambda})$.

The discussion in this section bases on a 2×2 MWH matrix, which describes two coupled harmonic oscillators,[61] i.e. one molecular vibrational mode Q (from out-of-cavity) and one cavity mode:

$$\begin{pmatrix} \omega_m^2 & g \\ g & \omega_c'^2 \end{pmatrix}. \tag{19}$$

We assume that the parameters ($\boldsymbol{\mu}^Q$ and $\boldsymbol{\alpha}$) in Eq.19 are from *ab initio* calculations of a molecule out-of-cavity. And it also worth noting that $\boldsymbol{\mu}^Q$ should be mass-weighted like in the Eq.17. The expression of coupling is $g = -\omega_c \boldsymbol{\lambda} \cdot \boldsymbol{\mu}^Q$. Its strength depends on the dot product between coupling vector $\boldsymbol{\lambda}$ and transition dipole $\boldsymbol{\mu}^Q$ of molecule vibrational mode Q. Again, $\omega_c'^2 = \omega_c^2 - \omega_c \boldsymbol{\lambda} \cdot \boldsymbol{\mu}^q$, in which $\boldsymbol{\mu}^q$ is the derivative of total dipole with respect to photon displacement, or the "transition dipole" of cavity mode.

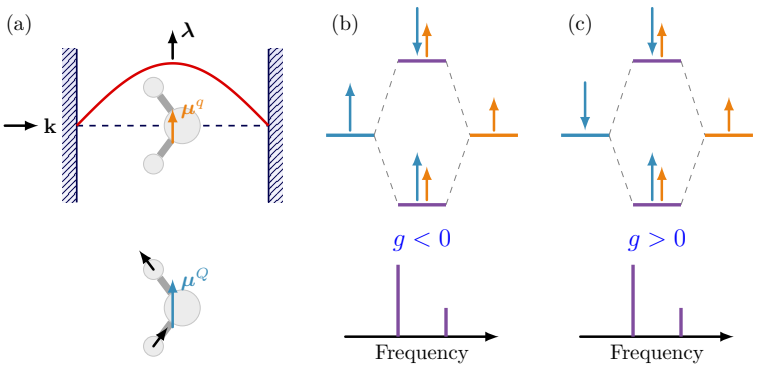

FIG. 2. (a) $\boldsymbol{\mu}^q$ interpreted as the induced dipole due to $\boldsymbol{\lambda}$, and transition dipole $\boldsymbol{\mu}^Q$ of the molecule vibrational mode. (b) and (c) The interaction diagrams of molecule vibration and cavity mode (above part), and the corresponding vibro-polaritonic spectra (lower part).

The vibro-polaritonic spectra is obtained by diagonalizing the interaction matrix in Eq.19. At first, we assume the resonance case of $\omega_m = \omega_c'$, indicating that the detuning is zero. Therefore the transition dipoles of upper polaritonic (UP) state and lower polaritonic (LP) state are combinations of $\boldsymbol{\mu}^Q$ and $\boldsymbol{\mu}^q$ of equal weight as shown in Fig.2. (The quantum and classical descriptions of coupled harmonic oscillators can be mapped to each other as shown in the supplementary material and Ref. 61.) It is interesting to see that no matter what the coupling value of g takes, the IR spectral intensity of LP state is always larger than that

of UP state. For example, if $g > 0$, which means that $\boldsymbol{\lambda}$ (i.e. $\boldsymbol{\mu}^q$) and $\boldsymbol{\mu}^Q$ are oriented in same direction, after diagonalization, the LP transition dipole is $\frac{1}{\sqrt{2}}(\boldsymbol{\mu}^q + \boldsymbol{\mu}^Q)$ and the UP transition dipole is $\frac{1}{\sqrt{2}}(\boldsymbol{\mu}^q - \boldsymbol{\mu}^Q)$. Therefore, the spectral intensity of LP state is larger than that of UP state at $g > 0$. If $g > 0$, meaning that $\boldsymbol{\lambda}$ ($\boldsymbol{\mu}^q$) and $\boldsymbol{\mu}^Q$ have opposite directions, then the LP and UP transition dipoles are $\frac{1}{\sqrt{2}}(\boldsymbol{\mu}^q - \boldsymbol{\mu}^Q)$ and $\frac{1}{\sqrt{2}}(\boldsymbol{\mu}^q + \boldsymbol{\mu}^Q)$, respectively. This implies that the spectral intensity of LP state is still larger than that of UP state at $g < 0$. So in resonance case, the spectral intensity of LP state is always larger than that of UP state.

In practical calculations, the cavity frequency ω_c (which appears in $\hat{H}_\mathrm{CBO}$) is often set equal to the frequency of one of molecular vibrations out-of-cavity. We consider $\boldsymbol{\mu}^Q$ and $\boldsymbol{\lambda}$ are oriented in the same direction so that we just represent them as scalars. The model Hessian is written as

$$\begin{pmatrix} \omega_\mathrm{c}^2 & -\omega_\mathrm{c}\lambda\mu^Q \\ -\omega_\mathrm{c}\lambda\mu^Q & \omega_\mathrm{c}^2 - \omega_\mathrm{c}^2\alpha\lambda^2 \end{pmatrix}. \tag{20}$$

Diagonalizing the model Hessian (details are shown in the supplementary material), the frequency and transition dipole of UP state are

$$\omega_+ = \left[\omega_\mathrm{c}^2 - \frac{(\mu^Q)^2}{\alpha}\tilde{\lambda}^2\sin^2\theta_0 - \frac{(\mu^Q)^2}{\alpha}\tilde{\lambda}\sin 2\theta_0\right]^{1/2}, \tag{21}$$

$$\mu_+ = \mu^Q\cos\theta_0 + \mu^q\sin\theta_0 = \mu^Q(\cos\theta_0 + \tilde{\lambda}\sin\theta_0), \tag{22}$$

and the frequency and transition dipole of LP state are

$$\omega_- = \left[\omega_\mathrm{c}^2 - \frac{(\mu^Q)^2}{\alpha}\tilde{\lambda}^2\cos^2\theta_0 + \frac{(\mu^Q)^2}{\alpha}\tilde{\lambda}\sin 2\theta_0\right]^{1/2}, \tag{23}$$

$$\mu_- = \mu^Q\sin\theta_0 - \mu^q\cos\theta_0 = \mu^Q(\sin\theta_0 - \tilde{\lambda}\cos\theta_0). \tag{24}$$

In the above equations, we define a dimensionless auxiliary variable $\tilde{\lambda} = \lambda/\left(\frac{\mu^Q}{\omega_\mathrm{c}\alpha}\right)$, and the optimal rotating angle $\theta_0 = \frac{1}{2}\tan^{-1}(-2/\tilde{\lambda})$. The results are plotted in Fig.3. In the left figure, as the strength of $\boldsymbol{\lambda}$ increases (characterized by $\tilde{\lambda}$ in the figures), the splitting between LP and UP states becomes larger. However we can see that the blue-shift of UP state eventually converges while the LP state continues to red-shift. The spectral intensities of UP and LP states are shown in the right figure. At the beginning ($\tilde{\lambda} = 0$), UP and LP states share equal spectral intensity. For non-zero $\tilde{\lambda}$, we find the result is similar to the previous paragraph: the intensity of LP state is always greater than that of UP state. And the peak of UP state even approaches to zero if $\tilde{\lambda}$ is large.

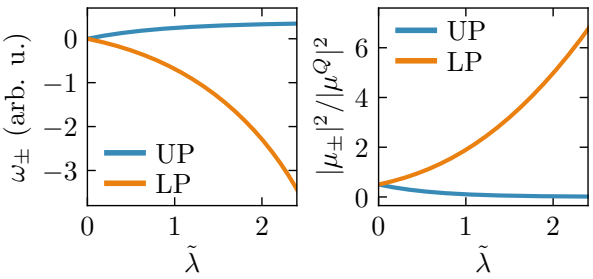

FIG. 3. The evolution of vibro-polaritonic spectra with respect to $\tilde{\lambda}$ at the case of $\omega = \omega_{\mathrm{m}}$. Left and right panels separately show the peak positions and spectral intensities of UP and LP states varied with $\tilde{\lambda}$.

The model Hessian presented in this section gives us a perspicuous picture to understand the cavity frequency shift and asymmetry peak in the *ab initio* vibro-polaritonic spectra. However the model Hessian neglects the interaction of cavity vacuum field on the molecules. First, the deformation of molecular geometry and the shift of molecular vibration frequency are neglected in the model. As shown in Ref. 46, the effective frequency of molecular vibration ω'_{m} is greater than the vibration frequency out-of-cavity ω_{m} due to the quadratic correction term with respect to $\boldsymbol{\lambda}$. We also assume that $\boldsymbol{\mu}^Q$ and $\boldsymbol{\alpha}$ do not vary with the strength of $\boldsymbol{\lambda}$. But since they depend on the electronic wavefunction (and nuclear configurations), this assumption becomes less appropriate when the strength of $\boldsymbol{\lambda}$ is large.

In CBO-DFT, the light-matter interaction is included, and the dependence of electronic state on cavity vacuum field is also considered. And in most cases, we will re-optimize the molecular geometry. Therefore, compared to the model Hessian, the *ab initio* method CBO-DFT and its analytical derivatives presented in this work allow us to adequately describe the vibro-polariton in the VSC regime.

As for Raman scattering spectra, the contribution to polarizability derivative from cavity mode $\boldsymbol{\alpha}^q$ is also considered. Following the same argument, $\boldsymbol{\alpha}^q$ corresponds to the first-order (static) hyperpolarizability, i.e. $\alpha^q_{mn} = \omega_{\mathrm{c}} \sum_l \lambda_l \beta_{mnl}$. To realize vibro-polariton, the relative orientation of $\boldsymbol{\lambda}$ and $\boldsymbol{\mu}^Q$ should be consistent to achieve strong coupling. And this explains the features that emerge in IR spectra. However for Raman spectra, the relation between $\boldsymbol{\alpha}^Q$ and $\boldsymbol{\alpha}^q$ is not so clear as in the case of dipole. The features of Raman scattering spectra of vibro-polariton may be system-dependent.

C. Vibro-Polaritonic Spectra of Acetone

In this section, we study the vibro-polariton formed by C−O stretching vibration of acetone and cavity mode. All calculations are performed at the theoretical level of B3LYP/def2-ma-SVP[62]. The spectral lineshapes are broadened using Lorentz distribution function, with full width at half maximum (FWHM) being $10\,\mathrm{cm}^{-1}$. For acetone out-of-cavity, the vibration frequency of C−O stretching is $1805.34\,\mathrm{cm}^{-1}$. As show in Fig.4, the C−O stretching mode is both IR and Raman active.

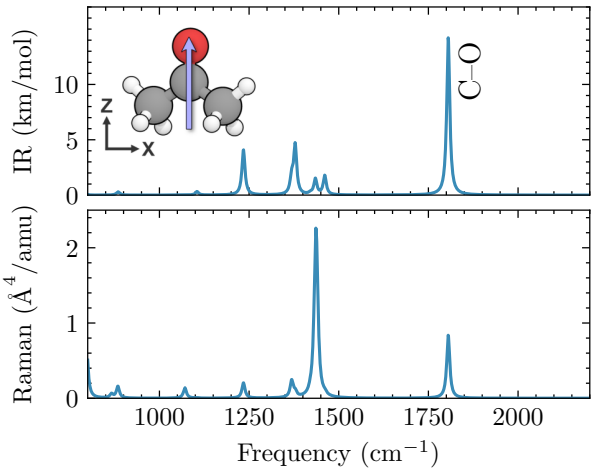

FIG. 4. The calculated IR (above) and Raman scattering (below) spectra of acetone out-of-cavity. The blue arrow shows the polarization direction of $\boldsymbol{\lambda}$.

For acetone in the cavity, we set cavity frequency $\omega_\mathrm{c} = 1805.34\,\mathrm{cm}^{-1}$, and $\boldsymbol{\lambda}$ is polarized along the C−O stretching direction (z-axis). The geometry of acetone and photon displacement coordinate q are all optimized. First we consider λ being 0.02, and the calculated vibro-polaritonic spectra (IR and Raman) are shown in Fig.5. The top panel in column (a) is the IR peak of C−O stretching out-of-cavity, and the cavity frequency we set is represented by the dashed line. In the second panel, we can see the effective vibration frequency of C−O stretching is slightly blue-shifted, and its IR intensity is nearly unchanged. The red-shift of cavity frequency is distinct ($\omega_\mathrm{c}' = 1789.752\,\mathrm{cm}^{-1}$), and the intensity of cavity peak is strong enough that can not be ignored. The IR spectra of vibro-polaritons are plotted in the lowest panel. The Rabi splitting between LP and UP states is $52.64\,\mathrm{cm}^{-1}$, and the central frequency of two peaks is $1799.92\,\mathrm{cm}^{-1}$. As expected, the vibro-polaritonic IR spectra is asymmetric, and the intensity of LP peak is stronger than that of UP peak. The

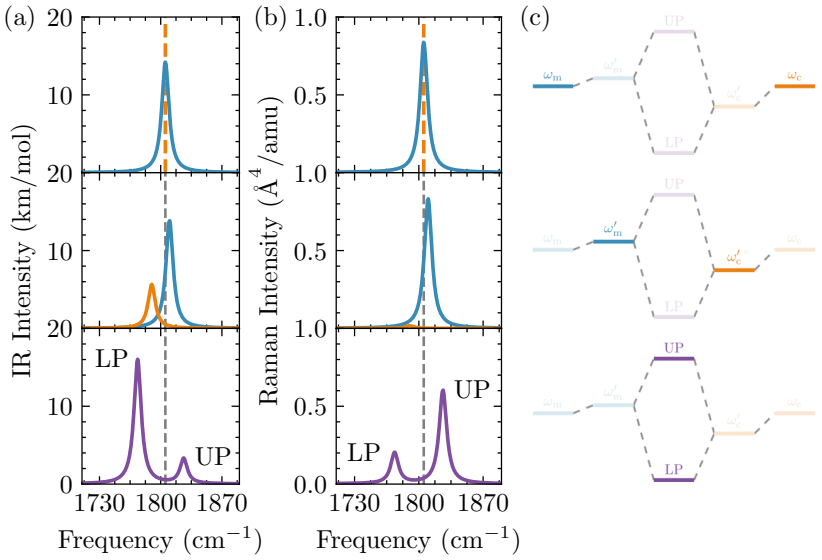

FIG. 5. The formation of vibro-polaritons and their IR and Raman spectra. (a) and (b) The IR and Raman spectra around the C=O vibration in the case of out-of-cavity (top) and in the cavity (bottom). The vibration mode and the naked cavity photon mode are presented as energy level in (c). In the cavity, the effective vibration frequency of molecule ω'_{m} is blue-shifted, while the frequency of cavity photon ω'_{c} is red-shifted. In the VSC regime, the hybrid vibro-polaritonic states are formed, leading to the lower-polariton (LP) and upper polariton (UP).

Raman spectra are presented in the second column. In contrast to IR spectra, the Raman scattering intensity of C−O stretching decreases in the cavity, and the contribution from the cavity is very small. The Raman spectra of vibro-polariton is also asymmetric, but in this case the peak of UP is higher. This is due to that the UP state has more molecule character (68.9 %).

Next we compare the IR spectra calculated by CBO-DFT and the model Hessian approach with respect to different value of $\boldsymbol{\lambda}$. The strength of $\boldsymbol{\lambda}$ includes 0.005, 0.01, 0.02, 0.04, and 0.06. In the model Hessian, the parameters $\boldsymbol{\alpha}$ and $\boldsymbol{\mu}^Q$ come from the calculation of acetone out-of-cavity. As for CBO-DFT, the parameters $\boldsymbol{\alpha}$ and $\boldsymbol{\mu}^Q$ in calculating the dimensionless $\tilde{\lambda}$ are from the CBO-DFT calculations with corresponding $\boldsymbol{\lambda}$. The results are plotted in Fig.6. It is shown that when the strength of $\boldsymbol{\lambda}$ is weak, the model Hessian can provide a good approximation of the vibro-polaritonic spectra. However, as the strength of $\boldsymbol{\lambda}$ increases, the deviation of model Hessian from the *ab initio* approach becomes apparent. The deviation of frequency of UP state is larger, mainly attributed to neglecting the shift of molecule effective

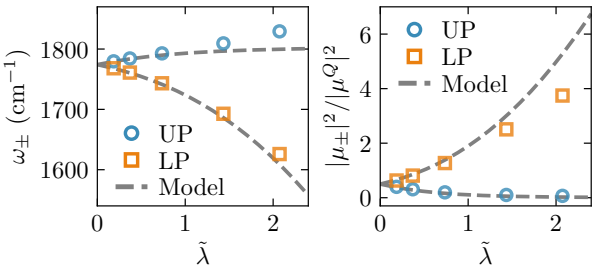

FIG. 6. The frequencies (left panel) and IR intensities (right panel) of vibro-polartions calculated by CBO-DFT and the model Hessian (dashed lines), respectively.

vibration frequency. For LP state, the error of transition dipole predicted by model Hessian is greater, and the source of error is that the changes of $\boldsymbol{\mu}^q$ (the main factor), $\boldsymbol{\alpha}$, and $\boldsymbol{\mu}^Q$ are not considered in model Hessian (the values of these quantities calculated at different strength of $\boldsymbol{\lambda}$ are plotted in the supplementary material).

Since we do not develop a model Hessian for the Raman spectra of vibro-polaritons, here we just show the Raman scattering factor of vibro-polaritons calculated by CBO-DFT, which are plotted in the Fig.7 as the ratio relative to the Raman scattering factor of C−O stretching out-of-cavity. In this example, the Raman intensity of UP state is always larger than that of LP state. Because $\omega'_{\mathrm{m}} > \omega'_{\mathrm{c}}$, the upper polariton has more molecule character so that its Raman intensity is stronger (contribution from cavity photon is marginal). When the strength of $\boldsymbol{\lambda}$ is relatively weak (< 0.02), the increase in the Raman intensity of UP state and the decrease in the LP state are approximately linear. However when $\lambda > 0.02$, the change of Raman intensity of UP state is quite wired: the intensity is smaller at $\lambda = 0.06$ than at $\lambda = 0.04$. To understand this phenomenon, we plot the sum of Raman intensity of UP and LP states on the right side of Fig.7. The larger λ is, the smaller the sum of Raman intensities is (i.e. smaller magnitude of polarizability derivative). So in the case of acetone, it is found that the Raman scattering spectra is suppressed in VSC.

Fig.8 shows how vibro-polaritonic spectra vary with the cavity frequency (the original value of frequencies and spectral intensities are plotted in the supplementary material). The detuning of cavity frequency $\omega_{\mathrm{c}} - \omega_{\mathrm{m}}$ ranges from $-120\,\mathrm{cm}^{-1}$ to $120\,\mathrm{cm}^{-1}$ with a step size of $10\,\mathrm{cm}^{-1}$. In all calculations, we set $\lambda = 0.02$, and perform full geometry optimization. To see the effect of cavity photon contribution ($\boldsymbol{\mu}^q$ and $\boldsymbol{\alpha}^q$) to the spectral intensity, we also calculate the spectra where we artificially set $\boldsymbol{\mu}^q$ and $\boldsymbol{\alpha}^q$ to zero in the expression of

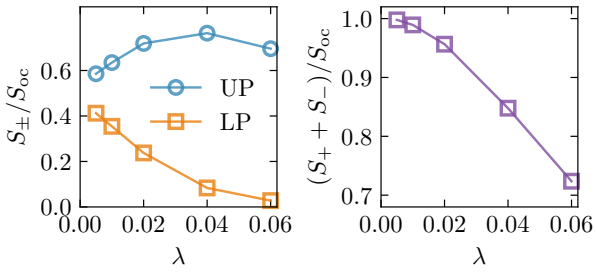

FIG. 7. Left: The ratio of Raman scattering factor between vibro-polariton $S_\pm$ and acetone out-of-cavity S_{oc} with respect to the strength of $\boldsymbol{\lambda}$. Right: Sum of the ratio changing with the strength of $\boldsymbol{\lambda}$.

spectral intensity (denoted as "without photon" in Fig.8). The horizontal dashed lines is the C−O stretching frequency out-of-cavity (1805.34 cm^{-1}), and the diagonal dashed lines is the cavity frequency we set. Near zero detuning, the well-known avoid-crossing pattern emerges. When the absolute value of detuning is larger, the molecule vibration and cavity mode do not effectively coupled. In IR spectra without cavity photon contribution, LP has the strongest IR intensity when there is large positive detuning; And when there is large negative detuning, UP has the strongest IR intensity. In both limits, the strong spectral

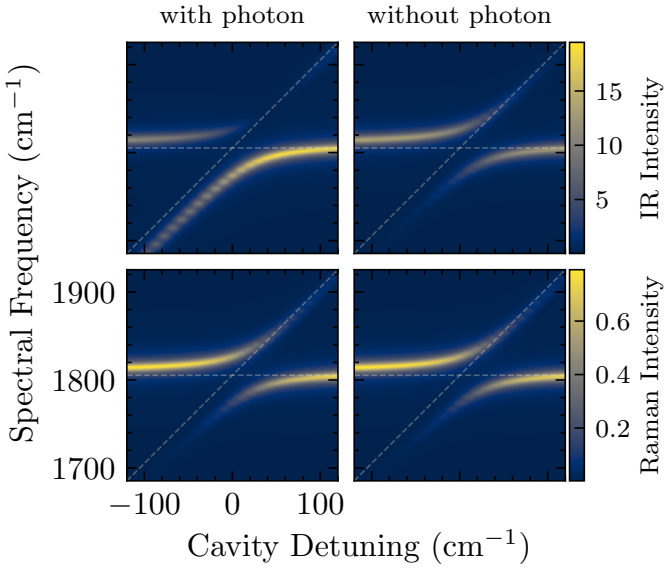

FIG. 8. IR and Raman spectra of vibro-polaritons varied with the cavity frequency detuning at $\lambda = 0.02$. "with photon" denotes including $\boldsymbol{\mu}^q$ and $\boldsymbol{\alpha}^q$ when calculating spectral intensities, and "without photon" means setting $\boldsymbol{\mu}^q$ and $\boldsymbol{\alpha}^q$ to zero when calculating spectral intensities.

intensity is due to their pure molecule character. For UP and LP, their spectral intensities gradually decrease to zero as their molecule character transforms into photon character. When photon contribution is considered as we do in CBO-DFT, the changing of IR intensity is not monotonic for both LP and UP. The maximum value of the IR intensity of LP appears at the detuning of $40\,\mathrm{cm}^{-1}$, while there is a minimum point (close to zero) in the IR intensity of UP at the same detuning. Of course this is due to the linear combinations of $\boldsymbol{\mu}^Q$ and $\boldsymbol{\mu}^q$, in which they cancel out in UP state, and most effectively coincide in LP state. As for Raman spectra, since the contribution of cavity photon itself is very small, the scanned spectra with or without photon are identical. The overall pattern is also similar to the IR spectra without photon contribution.

In the experimental setup, VSC is usually achieved by increasing the number of molecules in the cavity. In this part, we compare the vibro-polaritonic spectra of molecular ensemble containing N acetone molecules calculated by three approaches, with the assumption that all molecules have the same orientation, and the inter-molecular interaction and vibrational coupling are negligible. The first is to directly do *ab initio* CBO-DFT calculation for N molecules with the strength of coupling vector being λ_N (denoted as full CBO-DFT). The second is to perform CBO-DFT calculation for a single molecule with effective coupling vector $\lambda_{\text{eff}} = \sqrt{N}\lambda_N$ (denoted as effective coupling). The third calculation follows the idea of model Hessian: CBO-DFT is performed for a single molecule with λ_N, which gives an intermediate MWH $\tilde{\mathbf{H}}$. Then the model Hessian for N-molecular ensemble is built as

$$N\left\{\begin{array}{cccccc} \omega'^2_{\mathrm{m},1} & 0 & & & & g'_1 \\ 0 & \ddots & & & & \vdots \\ & & \omega'^2_{\mathrm{m},1} & 0 & & g'_1 \\ & & 0 & \ddots & & \vdots \\ & & & & \ddots & \vdots \\ g'_1 & \cdots & g'_1 & \cdots & \cdots & \omega'^2_{\mathrm{c},N} \end{array}\right., \tag{25}$$

in which the molecular part of $\tilde{\mathbf{H}}$ and the corresponding coupling are duplicated for N times. Since the polarizability (and hyperpolarizability) of N non-interacting molecules is expected to be N times that of a single molecule, we should artificially scale $\boldsymbol{\mu}^q$ and $\boldsymbol{\alpha}^q$ by N, and therefore the effective cavity frequency is $\omega'^2_{\mathrm{c},N} = \omega_{\mathrm{c}}^2 - N\omega\boldsymbol{\lambda}_N \cdot \boldsymbol{\mu}^q$. We consider an ensemble of nine acetone molecules that are uniformly stacked along the y-direction and separated

by 50 Å. The strength of coupling vector for molecular ensemble is $\lambda_N = 0.02/\sqrt{9}$, and the effective coupling vector is $\lambda_{\text{eff}} = 0.02$. The IR and Raman spectra calculated using three methods are shown in Fig.9. For comparison, the spectral intensities calculated by full CBO-DFT and model Hessian are divided by 9. All three methods produce similar results. However, with effective coupling method, due to the larger coupling vector, the effective molecular vibration frequency is more blue-shifted. This causes the deviation of spectral peak of UP state.

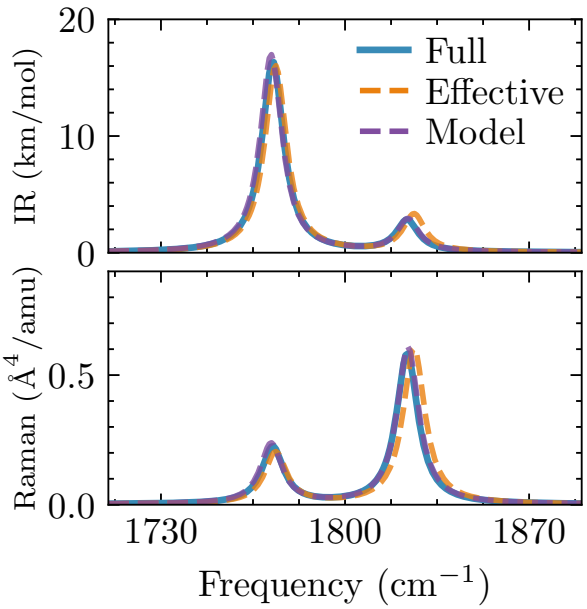

FIG. 9. The vibro-polaritonic IR and Raman spectra of acetone ensemble containing nine molecules in the cavity. "Full" stands for full CBO-DFT calculation, and the strength of coupling vector is set to be $\lambda_N = 0.02/\sqrt{9}$; "Effective" represents effective coupling method, in which the effective coupling vector $\lambda_{\text{eff}} = 0.02$ is used for calculating a single acetone; "Model" stands for model Hessian method, in which $\lambda_N = 0.02/\sqrt{9}$ is set for a single acetone.

This example tells that we are able to easily calculate the system with 90 nuclear DOFs by using analytic Hessian of CBO-DFT, and the model Hessian method provides a good approximation to the vibro-polaritonic spectra of molecular ensemble. Combining the advantages of both methods, calculating the vibro-polaritonic spectra of the ensemble of larger molecule are also feasible. The extra cost of model Hessian method is building the N-molecular ensemble Hessian and diagonalizing this bigger Hessian matrix, but they would not be a computational bottleneck. Although the effective coupling method has the low-

est computational cost, it overestimates the interaction of cavity acting on the molecular ensemble.

IV. CONCLUSIONS

By combining the CBOA with DFT, we have developed the CBO-DFT approach. Subsequently, we have formulated the analytical energy gradient and Hessian as well as the nuclear and photonic derivatives of dipole and polarizability within the framework of CBO-DFT. In addition, the geometry optimization on the CPES which involves nuclear and photonic DOFs has also been implemented. The successful implementation of these analytical derivatives and geometry optimization procedure into the electronic structure software package enable us to effectively calculate the geometric and spectral properties of vibro-polaritons and explore the critical points of CPES. By comparing the expression of the photonic derivative of dipole $\boldsymbol{\mu}^q$ and polarizability $\boldsymbol{\alpha}$, we find the important relation of $\boldsymbol{\mu}^q = \omega_c \boldsymbol{\alpha} \cdot \boldsymbol{\lambda}$. Therefore, $\boldsymbol{\mu}^q$ can be regarded as the induced dipole of molecule under the interaction of cavity electric field.

We also proposed a model Hessian to analyze how the vibro-polaritonic spectra varies with the increase of coupling strength $\boldsymbol{\lambda}$. It is found that the effective cavity frequency is always red-shifted, and the IR intensity of LP state is stronger than that of UP state. We demonstrate our implementation of CBO-DFT and compare the spectra of the acetone molecule in the cavity calculated by *ab initio* CBE-DFT and the model Hessian approaches. It is observed that both approaches produce the consistent results in relatively weak coupling regime. However, the deviation of model Hessian from the *ab initio* calculations becomes large when λ is great, attributed to the neglect of the photon-electron correlation in model Hessian. The Raman spectra of acetone in the cavity also show unexpected results: The Raman scattering factor of UP increases with λ when $\lambda < 0.04$, but it decreases when $\lambda = 0.06$. This is because the magnitude of the derivative of polarizability is suppressed at large value of λ, which also ascribes to the photon-electron correlation. In the framework of *ab initio* CBO, as we consider the contribution of $\boldsymbol{\mu}^q$ to the IR intensity of vibro-polaritons, the changing of spectral intensity with respect to the cavity detuning is not monotonic for both LP and UP. At last, we compare the vibro-polaritonic spectra of molecular ensemble calculated by three methods. The full CBO-DFT and model Hessian approaches produce

well-superposed spectra lines. The effective coupling vector method also give a good approximation to the ensemble spectra, but it produces a slightly blue-shifted UP peak.

Although we have make clear most of the features of *ab initio* vibro-polaritonic spectra in the CBO framework, there are questions remaining to solve. For example, we calculated the Raman scattering spectra within CBO-DFT with respect to the static electric field, and we did not go into it in depth. To compare with the experimental Raman intensities, one has to compute the dynamic polarizability and its nuclear derivatives. This requires to combine the time-dependent DFT with CBO. In fact, there is no unified view on experimental[24,25,63] and theoretical[64–66] research on Raman scattering of vibro-polaritons. A throughout study of the vibro-polaritonic Raman spectra from the *ab initio* aspect is therefore necessary. These are the topics we would like to solve in the future work.

ACKNOWLEDGMENTS

The financial support from the National Natural Science Foundation of China (Grant Nos. 22173074, and 21833006) is grateful.

DATA AVAILABILITY STATEMENT

The data that support the findings of this study are available within the article and its supplementary material.

REFERENCES

[1]R. J. Thompson, G. Rempe, and H. J. Kimble, "Observation of normal-mode splitting for an atom in an optical cavity," Phys. Rev. Lett. **68**, 1132–1135 (1992).

[2]R. Miller, T. E. Northup, K. M. Birnbaum, A. Boca, A. D. Boozer, and H. J. Kimble, "Trapped atoms in cavity QED: Coupling quantized light and matter," J. Phys. B: At. Mol. Opt. Phys. **38**, S551 (2005).

[3]B. M. Weight, X. Li, and Y. Zhang, "Theory and modeling of light-matter interactions in chemistry: Current and future," Phys. Chem. Chem. Phys. **25**, 31554–31577 (2023).

[4]B. S. Simpkins, A. D. Dunkelberger, and I. Vurgaftman, "Control, modulation, and analytical descriptions of vibrational strong coupling," Chem. Rev. **123**, 5020–5048 (2023).

[5]X. Huang, W. Zhang, and W. Liang, "Time-dependent Kohn-Sham electron dynamics coupled with nonequilibrium plasmonic response via atomistic electromagnetic model," J. Chem. Phys. **160**, 214106 (2024).

[6]X. Huang and W. Liang, "Real-time simulation of ultrafast electronic dynamics of nanoscale systems involving an organic molecule and a nanoparticle dimer," J. Phys. Chem. Lett. **15**, 6592–6597 (2024).

[7]K. Nagarajan, A. Thomas, and T. W. Ebbesen, "Chemistry under vibrational strong coupling," J. Am. Chem. Soc. **143**, 16877–16889 (2021).

[8]F. J. Garcia-Vidal, C. Ciuti, and T. W. Ebbesen, "Manipulating matter by strong coupling to vacuum fields," Science **373**, eabd0336 (2021).

[9]T. E. Li, B. Cui, J. E. Subotnik, and A. Nitzan, "Molecular polaritonics: Chemical dynamics under strong light-matter coupling," Annu. Rev. Phys. Chem. **73**, 43–71 (2022).

[10]W. Xiong, "Molecular vibrational polariton dynamics: What can polaritons do?" Acc. Chem. Res. **56**, 776–786 (2023).

[11]J. Lather and J. George, "Improving enzyme catalytic efficiency by co-operative vibrational strong coupling of water," J. Phys. Chem. Lett. **12**, 379–384 (2021).

[12]J. Lather, A. N. K. Thabassum, J. Singh, and J. George, "Cavity catalysis: Modifying linear free-energy relationship under cooperative vibrational strong coupling," Chem. Sci. **13**, 195–202 (2022).

[13]A. Thomas, J. George, A. Shalabney, M. Dryzhakov, S. J. Varma, J. Moran, T. Chervy, X. Zhong, E. Devaux, C. Genet, J. A. Hutchison, and T. W. Ebbesen, "Ground-state chemical reactivity under vibrational coupling to the vacuum electromagnetic field," Angew. Chem. Int. Ed. **55**, 11462–11466 (2016).

[14]R. M. A. Vergauwe, A. Thomas, K. Nagarajan, A. Shalabney, J. George, T. Chervy, M. Seidel, E. Devaux, V. Torbeev, and T. W. Ebbesen, "Modification of enzyme activity by vibrational strong coupling of water," Angew. Chem. Int. Ed. **58**, 15324–15328 (2019).

[15]A. Thomas, L. Lethuillier-Karl, K. Nagarajan, R. M. A. Vergauwe, J. George, T. Chervy, A. Shalabney, E. Devaux, C. Genet, J. Moran, and T. W. Ebbesen, "Tilting a ground-state reactivity landscape by vibrational strong coupling," Science **363**, 615–619 (2019).

[16]Y. Pang, A. Thomas, K. Nagarajan, R. M. A. Vergauwe, K. Joseph, B. Patrahau, K. Wang, C. Genet, and T. W. Ebbesen, "On the role of symmetry in vibrational strong coupling: The case of charge-transfer complexation," Angew. Chem. Int. Ed. **59**, 10436–10440 (2020).

[17]A. Sau, K. Nagarajan, B. Patrahau, L. Lethuillier-Karl, R. M. A. Vergauwe, A. Thomas, J. Moran, C. Genet, and T. W. Ebbesen, "Modifying Woodward-Hoffmann stereoselectivity under vibrational strong coupling," Angew. Chem. Int. Ed. **60**, 5712–5717 (2021).

[18]A. Shalabney, J. George, J. Hutchison, G. Pupillo, C. Genet, and T. W. Ebbesen, "Coherent coupling of molecular resonators with a microcavity mode," Nat. Commun. **6**, 5981 (2015).

[19]A. D. Dunkelberger, B. T. Spann, K. P. Fears, B. S. Simpkins, and J. C. Owrutsky, "Modified relaxation dynamics and coherent energy exchange in coupled vibration-cavity polaritons," Nat. Commun. **7**, 13504 (2016).

[20]A. B. Grafton, A. D. Dunkelberger, B. S. Simpkins, J. F. Triana, F. J. Hernández, F. Herrera, and J. C. Owrutsky, "Excited-state vibration-polariton transitions and dynamics in nitroprusside," Nat. Commun. **12**, 214 (2021).

[21]R. Duan, J. N. Mastron, Y. Song, and K. J. Kubarych, "Isolating polaritonic 2D-IR transmission spectra," J. Phys. Chem. Lett. **12**, 11406–11414 (2021).

[22]B. Cohn, S. Sufrin, and L. Chuntonov, "Ultrafast vibrational excitation transfer on resonant antenna lattices revealed by two-dimensional infrared spectroscopy," J. Chem. Phys. **156**, 121101 (2022).

[23]G. Stemo, J. Nishiuchi, H. Bhakta, H. Mao, G. Wiesehan, W. Xiong, and H. Katsuki, "Ultrafast spectroscopy under vibrational strong coupling in diphenylphosphoryl azide," J. Phys. Chem. A **128**, 1817–1824 (2024).

[24]A. Shalabney, J. George, H. Hiura, J. A. Hutchison, C. Genet, P. Hellwig, and T. W. Ebbesen, "Enhanced Raman scattering from vibro-polariton hybrid states," Angew. Chem. Int. Ed. **54**, 7971–7975 (2015).

[25]W. M. Takele, L. Piatkowski, F. Wackenhut, S. Gawinkowski, A. J. Meixner, and J. Waluk, "Scouting for strong light-matter coupling signatures in Raman spectra," Phys. Chem. Chem. Phys. **23**, 16837–16846 (2021).

[26]K. S. Menghrajani, M. Chen, K. Dholakia, and W. L. Barnes, "Probing vibrational strong coupling of molecules with wavelength-modulated Raman spectroscopy," Adv. Opt. Mater. **10**, 2102065 (2022).

[27]F. Verdelli, J. J. P. M. Schulpen, A. Baldi, and J. G. Rivas, "Chasing vibro-polariton fingerprints in infrared and Raman spectra using surface lattice resonances on extended metasurfaces," J. Phys. Chem. C **126**, 7143–7151 (2022).

[28]M. Ruggenthaler, J. Flick, C. Pellegrini, H. Appel, I. V. Tokatly, and A. Rubio, "Quantum-electrodynamical density-functional theory: Bridging quantum optics and electronic-structure theory," Phys. Rev. A **90**, 012508 (2014).

[29]J. Flick, D. M. Welakuh, M. Ruggenthaler, H. Appel, and A. Rubio, "Light-matter response in nonrelativistic quantum electrodynamics," ACS Photonics **6**, 2757–2778 (2019).

[30]J. Yang, Q. Ou, Z. Pei, H. Wang, B. Weng, Z. Shuai, K. Mullen, and Y. Shao, "Quantum-electrodynamical time-dependent density functional theory within Gaussian atomic basis," J. Chem. Phys. **155**, 064107 (2021).

[31]J. McTague and I. Foley, Jonathan J., "Non-Hermitian cavity quantum electrodynamics-configuration interaction singles approach for polaritonic structure with *ab initio* molecular Hamiltonians," J. Chem. Phys. **156**, 154103 (2022).

[32]N. Vu, G. M. McLeod, K. Hanson, and A. E. I. DePrince, "Enhanced diastereocontrol via strong light-matter interactions in an optical cavity," J. Phys. Chem. A **126**, 9303–9312 (2022).

[33]T. S. Haugland, E. Ronca, E. F. Kjønstad, A. Rubio, and H. Koch, "Coupled cluster theory for molecular polaritons: Changing ground and excited states," Phys. Rev. X **10**, 041043 (2020).

[34]U. Mordovina, C. Bungey, H. Appel, P. J. Knowles, A. Rubio, and F. R. Manby, "Polaritonic coupled-cluster theory," Phys. Rev. Res. **2**, 023262 (2020).

[35]M. Castagnola, R. R. Riso, A. Barlini, E. Ronca, and H. Koch, "Polaritonic response theory for exact and approximate wave functions," WIREs Comput. Mol. Sci. **14**, e1684 (2024).

[36]J. Flick, M. Ruggenthaler, H. Appel, and A. Rubio, "Atoms and molecules in cavities, from weak to strong coupling in quantum-electrodynamics (QED) chemistry," Proc. Natl. Acad. Sci. U.S.A. **114**, 3026–3034 (2017).

[37]J. Flick, H. Appel, M. Ruggenthaler, and A. Rubio, "Cavity Born-Oppenheimer approximation for correlated electron-nuclear-photon systems," J. Chem. Theory Comput. **13**, 1616–1625 (2017).

[38]T. E. Li, J. E. Subotnik, and A. Nitzan, "Cavity molecular dynamics simulations of liquid water under vibrational ultrastrong coupling," Proc. Natl. Acad. Sci. U.S.A. **117**, 18324–18331 (2020).

[39]E. W. Fischer and P. Saalfrank, "Ground state properties and infrared spectra of anharmonic vibrational polaritons of small molecules in cavities," J. Chem. Phys. **154**, 104311 (2021).

[40]J. Bonini and J. Flick, "*Ab initio* linear-response approach to vibro-polaritons in the cavity Born-Oppenheimer approximation," J. Chem. Theory Comput. **18**, 2764–2773 (2022).

[41]T. Schnappinger, D. Sidler, M. Ruggenthaler, A. Rubio, and M. Kowalewski, "Cavity Born-Oppenheimer Hartree-Fock ansatz: Light-matter properties of strongly coupled molecular ensembles," J. Phys. Chem. Lett. **14**, 8024–8033 (2023).

[42]T. Schnappinger and M. Kowalewski, "*Ab initio* vibro-polaritonic spectra in strongly coupled cavity-molecule systems," J. Chem. Theory Comput. **19**, 9278–9289 (2023).

[43]S. Angelico, T. S. Haugland, E. Ronca, and H. Koch, "Coupled cluster cavity Born-Oppenheimer approximation for electronic strong coupling," J. Chem. Phys. **159**, 214112 (2023).

[44]M. R. Fiechter and J. O. Richardson, "Understanding the cavity Born-Oppenheimer approximation," J. Chem. Phys. **160**, 184107 (2024).

[45]E. W. Fischer and P. Saalfrank, "Beyond cavity Born-Oppenheimer: On nonadiabatic coupling and effective ground state Hamiltonians in vibro-polaritonic chemistry," J. Chem. Theory Comput. **19**, 7215–7229 (2023).

[46]E. W. Fischer, J. A. Syska, and P. Saalfrank, "A quantum chemistry approach to linear vibro-polaritonic infrared spectra with perturbative electron-photon correlation," J. Phys. Chem. Lett. **15**, 2262–2269 (2024).

[47]Y. Yamaguchi and H. F. Schaefer III, "Analytic derivative methods in molecular electronic structure theory: A new dimension to quantum chemistry and its applications to spectroscopy," in *Handbook of High-resolution Spectroscopy* (John Wiley Sons, Ltd, 2011).

[48]W. Liang, Z. Pei, Y. Mao, and Y. Shao, "Evaluation of molecular photophysical and photochemical properties using linear response time-dependent density functional theory with classical embedding: Successes and challenges," The Journal of Chemical Physics **156**, 210901 (2022).

[49]J. J. Foley, J. F. McTague, and A. E. DePrince, "*Ab initio* methods for polariton chemistry," Chem. Phys. Rev. **4**, 041301 (2023).

[50]V. Rokaj, D. M. Welakuh, M. Ruggenthaler, and A. Rubio, "Light-matter interaction in the long-wavelength limit: No ground-state without dipole self-energy," J. Phys. B: At.

Mol. Opt. Phys. **51**, 034005 (2018).

[51]T. Helgaker, "Gradient theory," in *Encyclopedia of Computational Chemistry* (John Wiley & Sons, Ltd, 2002).

[52]J. A. Pople, R. Krishnan, H. B. Schlegel, and J. S. Binkley, "Derivative studies in Hartree-Fock and Møller-Plesset theories," Int. J. Quantum Chem. **16**, 225–241 (1979).

[53]D. R. Maurice, *Single Electron Theories of Excited States*, Ph.D Thesis, University of California, Berkeley (1998).

[54]T. Helgaker, S. Coriani, P. Jørgensen, K. Kristensen, J. Olsen, and K. Ruud, "Recent advances in wave function-based methods of molecular-property calculations," Chem. Rev. **112**, 543–631 (2012).

[55]Z. Pei, Y. Mao, Y. Shao, and W. Liang, "Analytic high-order energy derivatives for metal nanoparticle-mediated infrared and Raman scattering spectra within the framework of quantum mechanics/molecular mechanics model with induced charges and dipoles," J. Chem. Phys. **157**, 164110 (2022).

[56]E. Wilson, J. Decius, and P. Cross, *Molecular Vibrations: The Theory of Infrared and Raman Vibrational Spectra* (Dover Publications, 1980).

[57]J. Neugebauer, M. Reiher, C. Kind, and B. A. Hess, "Quantum chemical calculation of vibrational spectra of large molecules—Raman and IR spectra for Buckminsterfullerene," J. Comput. Chem. **23**, 895–910 (2002).

[58]E. Epifanovsky, A. T. B. Gilbert, X. Feng, J. Lee, Y. Mao, N. Mardirossian, P. Pokhilko, A. F. White, M. P. Coons, A. L. Dempwolff, Z. Gan, D. Hait, P. R. Horn, L. D. Jacobson, I. Kaliman, J. Kussmann, A. W. Lange, K. U. Lao, D. S. Levine, J. Liu, S. C. McKenzie, A. F. Morrison, K. D. Nanda, F. Plasser, D. R. Rehn, M. L. Vidal, Z.-Q. You, Y. Zhu, B. Alam, B. J. Albrecht, A. Aldossary, E. Alguire, J. H. Andersen, V. Athavale, D. Barton, K. Begam, A. Behn, N. Bellonzi, Y. A. Bernard, E. J. Berquist, H. G. A. Burton, A. Carreras, K. Carter-Fenk, R. Chakraborty, A. D. Chien, K. D. Closser, V. Cofer-Shabica, S. Dasgupta, M. de Wergifosse, J. Deng, M. Diedenhofen, H. Do, S. Ehlert, P.-T. Fang, S. Fatehi, Q. Feng, T. Friedhoff, J. Gayvert, Q. Ge, G. Gidofalvi, M. Goldey, J. Gomes, C. E. González-Espinoza, S. Gulania, A. O. Gunina, M. W. D. Hanson-Heine, P. H. P. Harbach, A. Hauser, M. F. Herbst, M. Hernández Vera, M. Hodecker, Z. C. Holden, S. Houck, X. Huang, K. Hui, B. C. Huynh, M. Ivanov, A. Jász, H. Ji, H. Jiang, B. Kaduk, S. Kähler, K. Khistyaev, J. Kim, G. Kis, P. Klunzinger, Z. Koczor-Benda, J. H. Koh,

D. Kosenkov, L. Koulias, T. Kowalczyk, C. M. Krauter, K. Kue, A. Kunitsa, T. Kus, I. Ladjánszki, A. Landau, K. V. Lawler, D. Lefrancois, S. Lehtola, R. R. Li, Y.-P. Li, J. Liang, M. Liebenthal, H.-H. Lin, Y.-S. Lin, F. Liu, K.-Y. Liu, M. Loipersberger, A. Luenser, A. Manjanath, P. Manohar, E. Mansoor, S. F. Manzer, S.-P. Mao, A. V. Marenich, T. Markovich, S. Mason, S. A. Maurer, P. F. McLaughlin, M. F. S. J. Menger, J.-M. Mewes, S. A. Mewes, P. Morgante, J. W. Mullinax, K. J. Oosterbaan, G. Paran, A. C. Paul, S. K. Paul, F. Pavošević, Z. Pei, S. Prager, E. I. Proynov, A. Rák, E. Ramos-Cordoba, B. Rana, A. E. Rask, A. Rettig, R. M. Richard, F. Rob, E. Rossomme, T. Scheele, M. Scheurer, M. Schneider, N. Sergueev, S. M. Sharada, W. Skomorowski, D. W. Small, C. J. Stein, Y.-C. Su, E. J. Sundstrom, Z. Tao, J. Thirman, G. J. Tornai, T. Tsuchimochi, N. M. Tubman, S. P. Veccham, O. Vydrov, J. Wenzel, J. Witte, A. Yamada, K. Yao, S. Yeganeh, S. R. Yost, A. Zech, I. Y. Zhang, X. Zhang, Y. Zhang, D. Zuev, A. Aspuru-Guzik, A. T. Bell, N. A. Besley, K. B. Bravaya, B. R. Brooks, D. Casanova, J.-D. Chai, S. Coriani, C. J. Cramer, G. Cserey, I. DePrince, A. Eugene, J. DiStasio, Robert A., A. Dreuw, B. D. Dunietz, T. R. Furlani, I. Goddard, William A., S. Hammes-Schiffer, T. Head-Gordon, W. J. Hehre, C.-P. Hsu, T.-C. Jagau, Y. Jung, A. Klamt, J. Kong, D. S. Lambrecht, W. Liang, N. J. Mayhall, C. W. McCurdy, J. B. Neaton, C. Ochsenfeld, J. A. Parkhill, R. Peverati, V. A. Rassolov, Y. Shao, L. V. Slipchenko, T. Stauch, R. P. Steele, J. E. Subotnik, A. J. W. Thom, A. Tkatchenko, D. G. Truhlar, T. Van Voorhis, T. A. Wesolowski, K. B. Whaley, I. Woodcock, H. Lee, P. M. Zimmerman, S. Faraji, P. M. W. Gill, M. Head-Gordon, J. M. Herbert, and A. I. Krylov, "Software for the frontiers of quantum chemistry: An overview of developments in the Q-Chem 5 package," J. Chem. Phys. **155**, 084801 (2021).

[59]P. J. Stephens, F. J. Devlin, C. F. Chabalowski, and M. J. Frisch, "*Ab initio* calculation of vibrational absorption and circular dichroism spectra using density functional force fields," J. Phys. Chem. **98**, 11623–11627 (1994).

[60]R. A. Kendall, J. Dunning, Thom H., and R. J. Harrison, "Electron affinities of the first-row atoms revisited. Systematic basis sets and wave functions," J. Chem. Phys. **96**, 6796–6806 (1992).

[61]M. S. Rider and W. L. Barnes, "Something from nothing: Linking molecules with virtual light," Contemp. Phys. **62**, 217–232 (2021).

[62]M. Gray and J. M. Herbert, "Comprehensive basis-set testing of extended symmetry-adapted perturbation theory and assessment of mixed-basis combinations to reduce cost,"

J. Chem. Theory Comput. **18**, 2308–2330 (2022).

[63]B. Cohn, T. Filippov, E. Ber, and L. Chuntonov, "Spontaneous Raman scattering from vibrational polaritons is obscured by reservoir states," J. Chem. Phys. **159**, 104705 (2023).

[64]J. Del Pino, J. Feist, and F. J. Garcia-Vidal, "Signatures of vibrational strong coupling in Raman scattering," J. Phys. Chem. C **119**, 29132–29137 (2015).

[65]J. Del Pino, F. J. Garcia-Vidal, and J. Feist, "Exploiting vibrational strong coupling to make an optical parametric oscillator out of a Raman laser," Phys. Rev. Lett. **117**, 277401 (2016).

[66]A. Strashko and J. Keeling, "Raman scattering with strongly coupled vibron-polaritons," Phys. Rev. A **94**, 023843 (2016).